
Highly accurate and efficient deep learning paradigm for full-atom protein loop modeling with KarmaLoop

Tianyue Wang^{1#}, Xujun Zhang^{1#}, Odin Zhang^{1#}, Peichen Pan^{1,*}, Guangyong Chen^{2,*}, Yu Kang^{1,*}, Chang-Yu Hsieh^{1,*}, Tingjun Hou^{1,*}

¹Innovation Institute for Artificial Intelligence in Medicine of Zhejiang University, College of Pharmaceutical Sciences, Zhejiang University, Hangzhou 310058, Zhejiang, China

²Zhejiang Laboratory, Hangzhou 311100, Zhejiang, China

Abstract

Protein loop modeling is the most challenging yet highly non-trivial task in protein structure prediction. Despite recent progress, existing methods including knowledge-based, *ab initio*, hybrid and deep learning (DL) methods fall significantly short of either atomic accuracy or computational efficiency. Moreover, an overarching focus on backbone atoms has resulted in a dearth of attention given to side-chain conformation, a critical aspect in a host of downstream applications including ligand docking, molecular dynamics simulation and drug design. To overcome these limitations, we present KarmaLoop, a novel paradigm that distinguishes itself as the first DL method centered on full-atom (encompassing both backbone and side-chain heavy atoms) protein loop modeling. Our results demonstrate that KarmaLoop considerably outperforms conventional and DL-based methods of loop modeling in terms of both accuracy and efficiency, with the average RMSD improved by over two-fold compared to the second-best baseline method across different tasks, and manifests at least two orders of magnitude speedup in general. Consequently, our comprehensive evaluations indicate that KarmaLoop provides a state-of-the-art DL solution for protein loop modeling, with the potential to hasten the advancement of protein engineering, antibody-antigen recognition, and drug design.

1 Introduction

Loops are irregular segments in protein structures that often link two regular secondary structures such as alpha helices or beta sheets^{1,2}. These structures are typically situated near the surface of proteins³, positioned in a way to allow them to facilitate numerous essential biological functions⁴, including regulation of enzyme activity⁵⁻⁸, protein-protein interaction (PPI)⁹ and protein-ligand recognition¹⁰⁻¹². Given their

high flexibility, loops heavily influence the overall protein dynamics¹³, rendering loop prediction one of the most challenging yet indispensable tasks in protein modeling¹⁴. Furthermore, since over half of the experimentally determined structures in the RCSB Protein Data Bank (PDB)¹⁵ contain missing loops⁴, accurate modeling of loop structures is of high significance. Particularly, one of the specific tasks in protein loop modeling is the prediction of antibody complementarity determining region (CDR) H3 loops. Compared with other CDRs, H3 has much higher flexibility, rendering it the most challenging task in antibody modeling¹⁶. To address this issue, various computational methods including traditional methods (knowledge-based, *ab initio* and hybrid) and deep learning (DL) methods have been proposed.

Knowledge-based methods, such as FREAD¹⁷, LoopIng¹⁸, SuperLooper¹⁹, and DaReUS-Loop²⁰, rely on template repositories collected from pre-existing protein structures and perform modeling based on certain standards, such as structural similarity. For instance, FREAD performs database searching using the four rule-based filters based on anchor C_α separations and the environmentally constrained substitution score. LoopIng selects templates from the database by taking advantage of both sequence- and geometry-related features. SuperLooper provides the first online server for modeling globular and membrane protein loops, where the loop candidates are chosen by the standard of the RMSD of the stem atoms. DaReUS-Loop uses fragments from remote or unrelated proteins to complete loop modeling and filters by sequence similarity and conformational profile. These methods are widely used in loop modeling, particularly in cases where a comparable fragment is available in the template database. However, the modeling performance of these methods for novel structures (especially for long loops) would drop sharply without proper references, suggesting the accuracy of these methods is severely limited by the available templates^{21,22}.

Ab initio methods, including DISGRO¹, LEAP²³, Cyclic coordinate descent (CCD)^{24,25}, robotics-based kinematic closure (KIC)²⁶ and next-generation KIC (NGK)²⁷, offer advantages over knowledge-based methods due to their independence from templates and the ability to explore a broader conformational space. However, they need more computational resources than knowledge-based methods, and their computational cost increases exponentially with the loop length²¹. DISGRO, for instance, employs a chain growth sequential Monte Carlo sampling strategy for loop modeling, which has been described as an efficient computational method and particularly effective for modeling loops with 10-17 residues. CCD minimizes the distances between the backbone atoms of the C-terminal moving anchor and the corresponding atoms in the fixed anchor by adjusting one dihedral angle at a time. KIC utilizes a robotics-inspired local loop reconstruction method for loop modeling, achieving sub-angstrom accuracy. Among *ab initio* methods, NGK has been commonly regarded to be the state-of-the-art^{20,21}, as it combines intensification and annealing strategies and yields a four-fold improvement over standard KIC.

Hybrid methods, such as CODA²⁸ and Sphinx²², integrate both *ab initio* and knowledge-based methods to improve performance²⁰. CODA utilizes a combination of the knowledge-based approach FREAD and the *ab initio* method PETRA²⁹ for generating a consensus prediction that should satisfy a set of rule-based filters. Sphinx combines

FREAD and an in-house *ab initio* method that first selects potential fragments shorter than the length of loop to be modeled. Then, the *ab initio* method adjusts the length of the fragments to generate accurate decoys of the desired length.

With the continual development of computing resource³⁰, deep learning (DL) has become increasingly popular and has demonstrated its potential in predicting protein structures. For instance, AlphaFold³¹ that incorporates biological and physical information and utilizes multi-sequence alignments (MSA) to design a DL algorithm, achieves atomic-level accuracy and ranks first in the 14th Critical Assessment of Structure Prediction (CASP) competition. Likewise, RoseTTAFold³² utilizes a three-track neural network that simultaneously considers protein sequences, amino acid interactions, and structures to attain accuracy close to AlphaFold³³. However, both methods often face significant challenges in accurately modeling loop regions^{33,34}. The first DL method for loop modeling was proposed in 2019, which employs Convolutional Neural Networks (CNN)³⁵⁻³⁹ on the distance matrix to predict the pairwise distances of loop atoms for conformation reconstruction. However, this method exhibits lower predictive accuracy compared to NGK on multiple test datasets.

More recently, DeepH3⁴⁰ was introduced as an antibody CDR H3 loop modeling method⁴¹ using CNN to predict the inter-residue distances and orientations from antibody heavy and light chain sequence. Furthermore, DeepAb⁴², the updated version of DeepH3, has demonstrated improvements with the inclusion of a pre-trained antibody sequence model and an interpretable attention mechanism that focuses on important residue pairs to accurately predict the structures of antibodies. ABlooper⁴³ is another approach that utilizes the E(n) Equivariant Graph Neural Networks (EGNN)⁴⁴ architecture to predict the backbone atoms of antibody loops, but it is slightly less accurate than DeepAb.

So far, both traditional and DL-based methods have been unable to achieve high accuracy and efficiency simultaneously. Moreover, most proposed methods have focused solely on the heavy atoms of the backbone within the loop region^{1,24,45-49}. Nonetheless, it is crucial to predict the conformation of side chains accurately, especially in the context of protein-ligand docking⁵⁰⁻⁵², which highlights the significance of executing meticulous full-atom modeling of loops.

For the reasons above, we present a novel end-to-end DL paradigm named KarmaLoop, which is designed for accurate and efficient full-atom prediction of protein loops. Figure 1A depicts an example of a loop modeled by KarmaLoop which starts with a random initialization of the loop coordinates and then predicts an accurate loop structure. KarmaLoop (Figure 1B) deploys GNN architectures comprising two encoders (i.e., Graph Transformer⁵³⁻⁵⁵ (GT) and Geometric Vector Perceptrons⁵⁶ (GVP)) for intramolecular interaction encoding, a Mixture Density Network (MDN) block for obtaining confidence score, and an EGNN block for generating the conformation. The innovations are as follows: (1) protein residues and atoms are embedded hierarchically, and atom features are aggregated into the corresponding residues to attain a fusion representation (Figure 1C); (2) distribution of the minimum distance between loop and non-loop nodes fitted by the MDN block introduces an inductive bias to the shared encodes which can facilitate pose generation and confidence prediction; (3) self-attention-based EGNN with fully-connected interaction graphs is deployed to enable fast coordinates prediction;

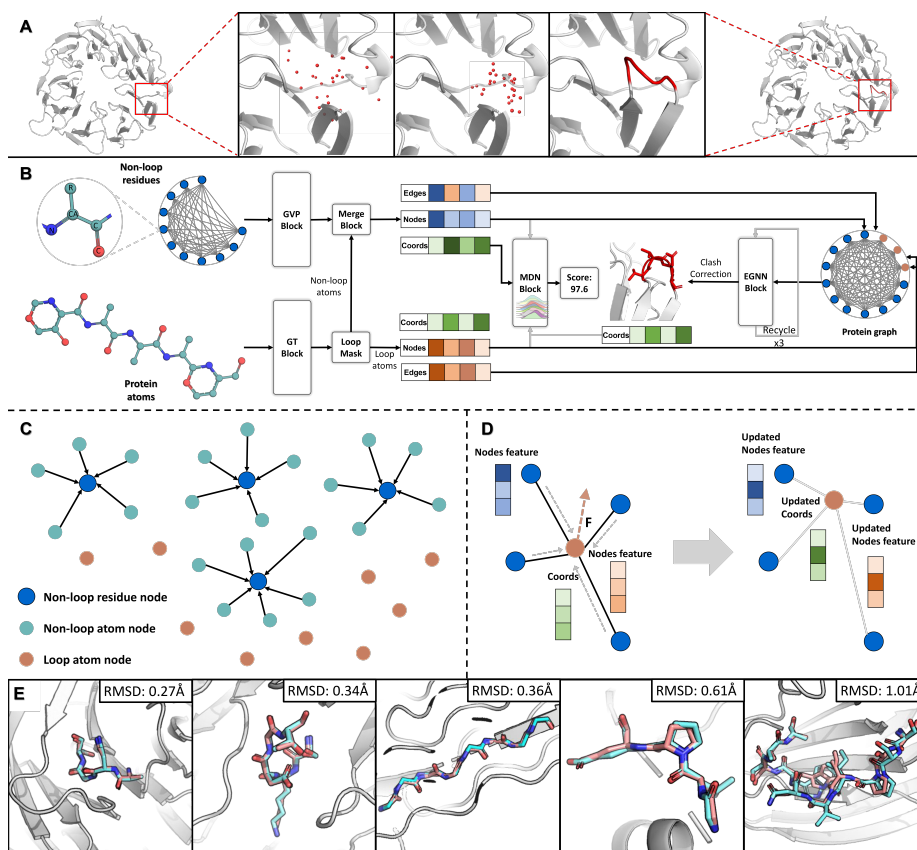


Figure 1. The workflow of KarmaLoop for loop modeling.

(4) a clash correction module is implemented to assist in forming chemically plausible conformations.

KarmaLoop has been evaluated on multiple benchmark datasets, including the general protein loop benchmark CASP13+14 (the combination of CASP13⁵⁷ and CASP14⁵⁸), the CASP15 dataset and the antibody H3 loop benchmark (RosettaAntibody and therapeutic benchmark used in DeepAb). In terms of the general protein loop modeling capability, KarmaLoop outperforms all the tested traditional and DL-based methods on both accuracy and efficiency, with the medium full-atom root-mean-square deviations (RMSDs) of 1.02 Å and 1.03 Å, the average RMSDs of 1.36 Å and 1.49 Å, the success rates of 81.9% and 83.9%, and the speeds of 0.047 seconds (s) and 0.049s per task on the CASP13+14 and CASP15 benchmark datasets, respectively. Several successful predictions of antibody CDR H3 loops are shown in Figure 1E, where KarmaLoop achieves the average full-atom and medium RMSDs of 2.09 Å and 2.24 Å respectively, compared with the baseline methods with the best performance (average and medium RMSDs of 3.40 Å and 3.74 Å, respectively). Additionally, when using the DeepAb-modeled antibody structures as the input, KarmaLoop could further refine the

conformations of H3 loops and increase the accuracy by 13.14% and 17.35% on the medium and average RMSDs, respectively. Hence, we proposed a universal protocol for precise antibody modeling by employing DeepAb to first predict an overall antibody structure, followed by KarmaLoop to refine the H3 loops. In summary, KarmaLoop has shown a remarkable superiority (over prior arts) in predicting both general loops and antibody H3 loops across most loop lengths.

2 Results and Discussion

2.1 Prediction accuracy for general protein loops

The accuracy of loop modeling is of utmost importance for many practical applications. To validate the capability of our model, 6 widely used methods including two DL-based methods (AlphaFold and RoseTTAFold), one knowledge-based method (FREAD), and three *ab initio* methods (DISGRO, NGK, and Rosetta model_missing_loop (RML)) were employed for comparison with KarmaLoop in a comprehensive benchmark. The full-atom RMSDs were calculated for each method with the AlphaFold and RoseTTAFold predicted structures being aligned before computation.

To perform quantitative comparisons with the other methods, empirical Cumulative Distribution Function (eCDF) was selected to describe the proportion of samples at given RMSD values. We defined a task as successful if the RMSD of a given sample falls below a specified threshold. Figure 2A&B demonstrates that when the RMSD threshold was set to 2 Å, KarmaLoop exhibited the highest success rates of 83.91% and 81.80%, respectively, on the CASP13+14 and CASP15 benchmark datasets, yielding significant improvements by 28.09% and 19.90% over the next best method (i.e., AlphaFold, 55.82% and 61.90%). Even adopting a stricter RMSD standard of 1 Å, KarmaLoop (46.71% and 49.38%) still outperformed the other methods, ranging from RoseTTAFold (2.55% and 1.26%) to NGK (21.69% and 23.26%). Of note, KarmaLoop achieved the success rates of 97.48% and 94.76%, respectively, on the two benchmark datasets when the threshold was set to 4 Å.

As some baseline methods may generate multiple conformations for a given loop sample, KarmaLoop was further evaluated in the context of generating multiple conformations (KarmaLoop generated one conformation while AlphaFold and RoseTTAFold produced 5 conformations and the other baseline methods outputted 10 conformations). It is important to note that, regardless of the number of conformations generated for a given task, a successful prediction is acknowledged when the lowest RMSD is less than 2 Å. As shown in Figure 2C, KarmaLoop achieved the best performance and improved the success rates by 13.27% and 9.94%, respectively, on the two benchmark datasets, compared with the best model NGK with the success rates of 70.64% and 71.36%, respectively. The performance of RoseTTAFold was the worst with the success rates of only 39.38% and 30.58%, respectively.

To directly compare the performance, the distribution of each method was plotted in Figure 2D. KarmaLoop showed the lowest medium RMSDs on the CASP13+14 and CASP15 datasets, with 1.03 Å and 1.02 Å, respectively, as compared to the other methods, and

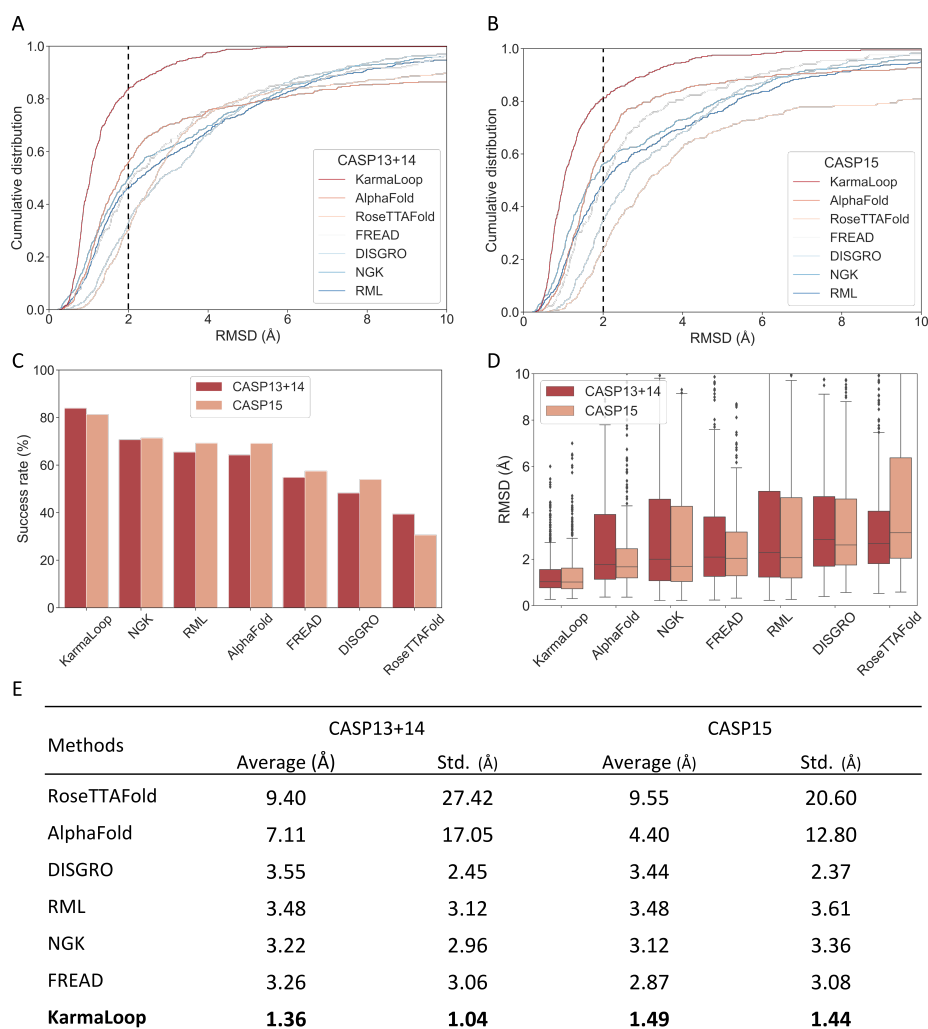


Figure 2. Performance of KarmaLoop and protein loop modeling methods on the CASP dataset. (A) Empirical cumulative distribution of RMSD of the tested methods on (A) the CASP13+14 dataset and (B) the CASP15 dataset, and the dashed line indicates the 2Å RMSD cut-off. (C) The success rate was calculated in the 2Å RMSD threshold, with KarmaLoop generating only **one** conformation, AlphaFold and RoseTTAFold generating **5** conformations and the other methods generating **10** conformations. (D) The RMSD distribution of the tested methods, and the red boxes indicate the CASP13+14 dataset and the salmon boxes indicate the CASP15 dataset. (E) The average and standard deviation (Std.) of the RMSDs of all the tested methods.

showed much lower RMSDs than the second-best method AlphaFold (1.77 Å and 1.67 Å). Besides, KarmaLoop achieved the average RMSD of 1.36 Å (± 1.04 Å) and 1.49 Å (± 1.44 Å), holding a significant leading margin of 57.76% and 52.24% over the next best baseline method NGK on the CASP13+14 and CASP15 datasets (Figure 2E).

2.2 The impact of loop length on accuracy

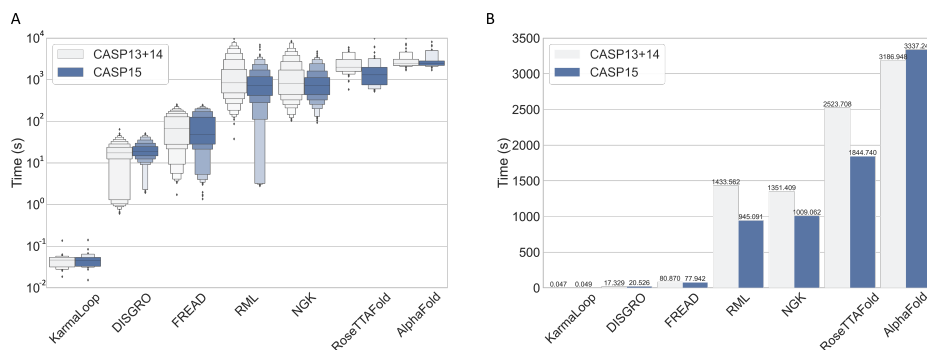


Figure 3. Performance of KarmaLoop and the other tested methods across various loop lengths. The performance tested on (A) the CASP13+14 benchmark dataset and (B) on the CASP15 dataset.

Long loop prediction has been an enduring challenge in loop modeling²¹. Therefore, we investigated the influence of loop length on prediction accuracy. As shown in Figure 1E, KarmaLoop could generate satisfactory conformations of loops with varying lengths. Figure 3A&B displayed the RMSDs of each loop length in the CASP13+14 and CASP15 datasets. Our results indicated that KarmaLoop outperformed the baseline methods for the majority of length cases (15/23 and 18/25 on the CASP13+14 and CASP15 datasets), and maintained a relatively consistent performance across different loop lengths. The RMSDs for most loops shorter than 10 residues were below 2.0 Å. As the loop length increased to 20 residues, the majority of the samples exhibited RMSDs less than or equal to 4.0 Å. Notably, the RMSDs were below 10 Å for almost all loop lengths, even for extremely long loops. The observed increase in RMSD with loop length may be attributed to the fact that the training dataset predominantly consisted of short loops (residues ≤ 10), and long loops (particularly those over 20 residues) were only represented by 0.058% of all the samples.

2.3 Evaluation of loop modeling efficiency.

Computational efficiency is also a key factor in loop modeling. In this section, the time consumption of each method was evaluated. KarmaLoop was tested on a Tesla V100S GPU, traditional methods (FREAD, DISGRO, NGK and RML) were run on a single core Intel(R) Xeon(R) Gold 6240R CPU @ 2.40GHz, and AlphaFold and RoseTTAFold were evaluated in parallel with 20 cores on the Intel(R) Xeon(R) Gold 6240R CPU @ 2.40GHz and a Tesla V100S GPU. Figure 4A shows the distribution of time spent for each method, illustrating the remarkable efficiency of KarmaLoop in terms of time cost on each task ranging from 0.015s to 0.14s. Contrastively, the time cost of DISGRO ranges from 0.611s to 64.36s, and the other methods are considerably slower. As shown in Figure 4B, the average time costs of KarmaLoop on the CASP13+14 and CASP15 datasets are 0.047s and 0.049s, respectively, displaying a considerable speed advantage over traditional methods. Specifically, the minimum speed advantages of KarmaLoop over DISGRO (17.329s and 20.526s) are 368 \times and 418 \times for CASP13+14 and CASP15,

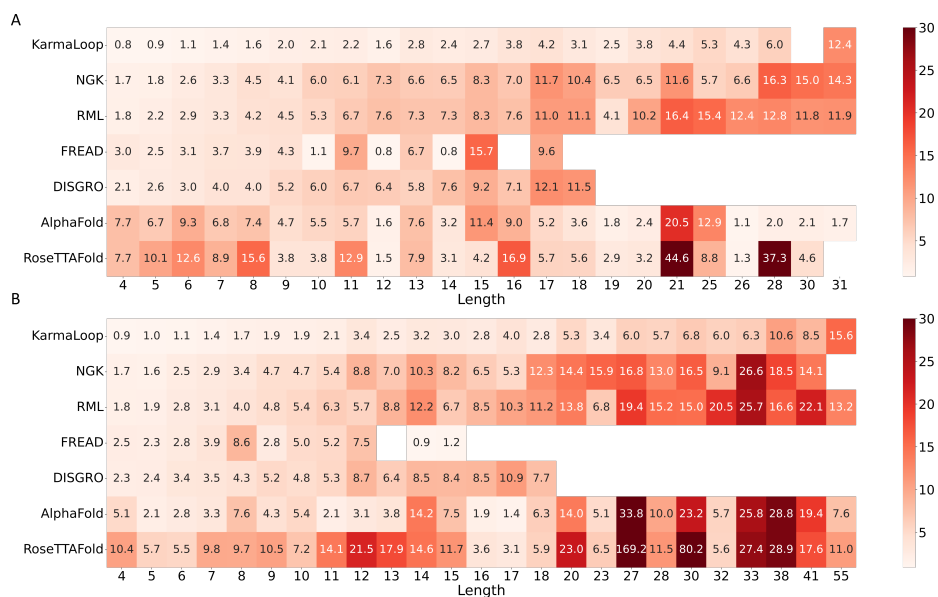


Figure 4. The time cost of each tested method. (A) Time distribution of each method. (B) Average time cost. Further details on the hardware setup can be found in the main text.

respectively, and the maximum speed advantages of KarmaLoop over RML (1433.562s and 945.091s) are 30,489 \times and 19,287 \times , respectively. However, it should be noted that unlike other methods that only model loop region, AlphaFold and RoseTTAFold require predicting the entire protein conformation. Thus, the modeling speed for these methods cannot be directly compared. While the reported speedup may vary slightly depending on the hardware used, the two to four orders of magnitude in speedup should still hold unless these baseline tools have been completely re-engineered to boost their efficiency.

2.4 Prediction of antibody H3 loops

The CDR H3 of antibody is widely acknowledged as the most flexible region⁵⁹ and contributes the most to the structural diversity and binding site topography¹⁶. Consequently, accurate modeling of the H3 conformation is urgently needed. Sphinx, proposed by Marks et al., is a hybrid method that models both general loops and antibody H3 loops with the same architecture but using different fragment databases²². In contrast, KarmaLoop consistently employs the same process for H3 modeling.

In this section, we present a comparative analysis of the H3 modeling performance of KarmaLoop against four widely used methods (i.e., DeepAb⁴², RosettaAntibody-G⁶⁰, RepertoireBuilder⁶¹, and AbodyBuilder⁶²) for predicting antibody structures on the antibody H3 benchmark. To evaluate the quality of the modeling results, we used the experimentally determined structures from SAbDab as the input. Figure 5A depicts the distribution of the RMSDs between the predicted samples from the baseline methods and the experimentally determined structures. The results demonstrate that KarmaLoop (2.09 Å, 2.24 Å) outperforms DeepAb

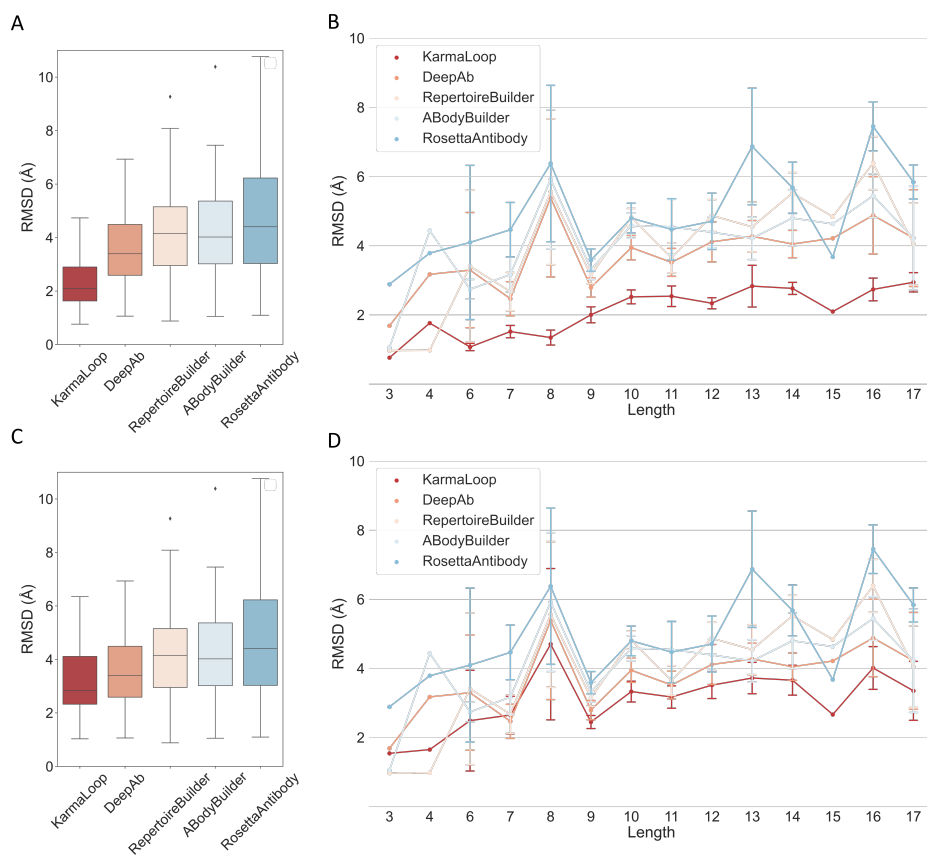


Figure 5. Comparison of the antibody CDR H3 loop prediction accuracy. (A) Distribution of the RMSD values for each method. (B) Average RMSDs of different lengths on the tested methods. The error bar shows the Std. of the corresponding length target. (C) Distribution of the RMSD values for each method (KarmaLoop makes refinement based on the antibody structures modeled by DeepAb). (D) Average RMSDs of different length on the tested methods (KarmaLoop makes refinement based on the antibody structures modeled by DeepAb).

(3.40 Å, 3.73 Å) in terms of the medium and average RMSDs by 1.31 Å and 1.49 Å, respectively. Figure 5B displays the RMSDs of samples with varying loop lengths, and KarmaLoop exhibits the lowest average RMSD for almost all lengths of H3 loop samples.

Next, we assessed the ability of refinement by using the DeepAb-predicted antibody structures as the input for KarmaLoop. Figure 5C&D illustrate the predictions based on the structures modeled by DeepAb, which can be used to test the capability of KarmaLoop to improve structures under a suboptimal structural situation. The results depicted in Figure 5C&D demonstrate that KarmaLoop is capable of refining the loop structures with an average RMSD reduction from 3.73 Å to 3.24 Å and a medium RMSD reduction from 3.40 Å to 2.81 Å, resulting in 13.14% and 17.35% improvement,

respectively. It is worth noting that this improvement is observed across most lengths of the H3 loops, highlighting the consistent ability of KarmaLoop to improve the H3 loop structures regardless of their length. Thus, a universal protocol can be applied for antibody prediction, whereby DeepAb models the entire antibody structures and KarmaLoop reconstructs the H3 structures.

2.5 Learning the principle of physical interactions

To elucidate the interpretability of KarmaLoop, we present a pair of case studies by portraying both covalent and non-covalent interactions. As exhibited in Figure 6A, the attention values between the start nodes and end nodes are displayed, which demonstrates the proficiency of KarmaLoop in apprehending the interactions between the anchor residues and the adjacent loop termini residues, a critical facet for the formation of loop conformation²². Figure 6B, on the other hand, illustrates the capacity of KarmaLoop to perceive non-covalent interactions, such as π -stacking, which are important in the genesis of internal loop conformation. Overall, these findings suggest that KarmaLoop is capable of capturing implicit interactions without the need for prior knowledge.

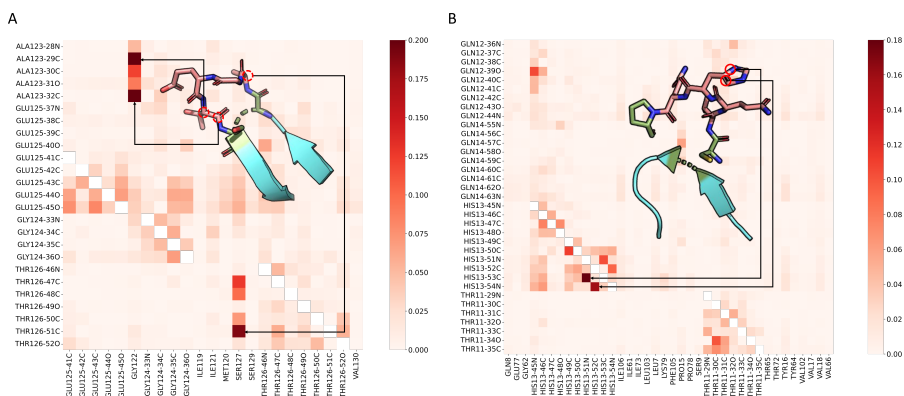


Figure 6. Attention weights in KarmaLoop. (A) Interactions between anchor residues (before or after loop region) and adjacent loop termini residues, the attention values increase with red gets deeper, pink represents the loop residues, green represents the anchor residues, blue is the non-loop and non-anchor region, and the red dashed circle indicates the atoms of loop residue that have interactions with anchor residues (PDB ID: T1071-D1 from CASP15). (B) Interactions of internal bonds of loop residues, the red circle indicates the bond between two atoms (PDB ID: T1066 from CASP14).

3 Conclusion

In this work, we introduced a novel DL paradigm, KarmaLoop, to predict and model protein loop conformations. KarmaLoop achieved sub-angstrom accuracy and high efficiency based on the following innovative components: (1) a hierarchical representation of residues and atoms to precisely characterize protein structures; (2) the use of MDN for learning pair-wise distances between loop and non-loop nodes to facilitate loop conformation generation; (3) the deployment of self-attention-based EGNN with fully-connected interaction graphs for fast coordinate prediction; (4) an integrated clash

correction procedure to enforce the generation of chemically plausible conformations.

To verify the effectiveness of KarmaLoop, several evaluations and comparisons have been conducted, including general loop modeling accuracy, loop-length impact and compute time, as well as potential applications in antibody H3 prediction. Of note, KarmaLoop achieved a significant improvement in the average RMSD by more than two-fold and the medium RMSD by nearly two-fold. Regarding the success rate, the minimum enhancement of 28.09% and 19.90% in the CASP13+14 and CASP15 benchmark datasets were observed on one conformation generated by each method. Even when compared to other methods that generate multiple conformations, KarmaLoop with only one generated conformation still achieved a minimum improvement of 13.27% and 9.94%. KarmaLoop is also capable of accurately modeling loops of different lengths, and obtained a majority length preponderance against the other methods. Surprisingly, KarmaLoop achieved at least a 368× speed advantage than other traditional methods. In term of antibody CDR H3 loop modeling, which is considered the most challenging task in antibody structure prediction, KarmaLoop also showed the best performance and maintained its superiority across various lengths. Notably, based on the DeepAb-modeled antibody structures, KarmaLoop has successfully promoted its accuracy and achieved improvement upon DeepAb in each length of H3 loop.

In summary, KarmaLoop has demonstrated the potential to accurately model loops, refine loop conformations based on inaccurate structure environments, and significantly accelerate batch data processing. Besides, a universal protocol was proposed for antibody structure prediction by utilizing DeepAb to model the entire structure of the antibody and KarmaLoop to refine the H3 conformation. Except for an accurate loop modeling paradigm proposed, a large training dataset (0.27 million) and several benchmark datasets have been made available for researchers to further evaluate the prediction accuracy of the general loop and antibody H3. We anticipate that KarmaLoop will accelerate the advancement of protein design, antibody-antigen recognition and drug discovery, and will become an essential tool in the field of biology moving forward.

Despite the considerable advancements achieved, KarmaLoop continues to exhibit certain limitations. The model currently only provides a single conformation, and there is a discernible decrease in accuracy when confronted with extremely long loops. To address these constraints in future development, two potential directions can be explored. First, designing a probabilistic model capable of generating multiple conformations might expand the competencies of model. Second, enriching the training data with additional long-loop samples could augment the model’s efficacy in handling complex long-loop tasks. These enhancements represent promising avenues for subsequent investigations.

4 Method

4.1 Architecture overview

Inspired by Jin⁶³, we consider the loop modeling problem as the docking task and selected any residues within 12 Å of loop atoms as the loop pocket, which is a common

and frequently used protocol for ligand docking⁵³. As depicted in Figure 1B, the entire protein pocket is characterized as a 2D molecular graph G_p , with atoms as nodes and covalent bonds as edges. The non-loop region of the protein is represented as a 3D residue graph G_{nl} with residues as nodes and edges connecting the top 30 nearest neighbor nodes, which captures long-range interactions better and has a lower computational cost than a graph with atoms as nodes.

Instead of directly being used as the inputs for downstream tasks, the molecular graphs and residue graphs are encoded by Graph Transformer⁵³⁻⁵⁵ (GT) and Geometric Vector Perceptrons⁵⁶ (GVP) to learn intra-molecular interactions and update node embeddings. Then, for non-loop residues, the node embeddings for atom nodes in the same residue are summed and concatenated to the corresponding residue node embeddings, followed by a feature merging block (FMB) to generate hierarchical node embeddings.

$$H_{p,s}^1 = GT(H_{p,s}^0, E_{p,s}^0) \quad (1)$$

$$H_{nl,s}^{0.5} = GVP(S_{nl,s}^0, H_{nl,s}^0, H_{nl,v}^0, E_{nl,s}^0, E_{nl,v}^0) \quad (2)$$

$$H_{nl,s,i}^1 = FMB\left(\text{concat}\left(H_{nl,s,i}^{0.5}, \sum_{j=k}^{k'} H_{p,s,j}^1\right)\right) \quad (3)$$

$$H_{l,s}^1 = H_{p,s}^1[\text{loop_mask}] \quad (4)$$

where H and E represent nodes and edges features, respectively; S represents the residue type; loop mask is a bool array for selecting loop atoms from the whole protein atoms; $p, nl, l, s, v, i, j, k, k'$ on the lower right (i.e. subscripts) denote protein pocket atoms, non-loop residues, loop residues, scalar, vector, the index of residues, the index of atoms, the start index of the atom corresponding to i th residue, and the end index of the atom corresponding to i th residue, respectively.

Then, the node embeddings $(H_{l,s}^1, H_{nl,s}^1)$ from the encoders and the node coordinates $(X_{l,s}^1, X_{nl,s}^1)$ of both the loop atoms and non-loop residues are combined to form an interaction graph $[G_{l,nl} = (H_{l,nl}, E_{l,nl}, X_{l,nl})]$, which captures inter-molecular interactions at both the residue-atom and atom-atom levels.

In the process of pose generation, the loop conformation, represented as the coordinates of the loop atom nodes, is initialized by sampling from the normal distribution with a mean around the pocket center and a standard deviation of 4 Å. The node embeddings and edge features are initialized by graph normalization and an MLP layer (formula 5). Then the node embeddings, edge embeddings and loop atoms positions are updated through the application of the EGNN block consisting of 8 EGNN layers with self-attention, taking into account both interactions between loop, non-loop and loop, loop interactions (equation 6). Inspired by AlphaFold, a recycling strategy is employed to enable the

EGNN block to learn how to consistently refine the poses. At the start of each recycling, the updated embeddings and the raw embeddings will be well combined through a gate block (equation 7).

$$H_{l,nl}^{0,0} = \text{GraphNorm}(H_{l,s}, H_{nl,s}) \quad (5)$$

$$H_{l,nl}^{r,i}, E_{l,nl}^{r,i}, X_{l,nl}^{r,i} = \text{EGNN_Layer}^i(H_{l,nl}^{r,i-1}, E_{l,nl}^{r,i-1}, X_{l,nl}^{r,i-1}) \quad (6)$$

$$F_{l,nl}^{r+1,0} = \text{Gate_Block}(F_{l,nl}^{r,8}, F_{l,nl}^{0,0}) \quad (7)$$

where H and E represent embeddings of node and edge, respectively; F refers to an embedding in general; l, nl, r and i represent loop atoms, non-loop residues, the recycling index and the EGNN layer index, respectively.

Upon obtaining node embeddings, the MDN block is used to predict essential statistical parameters such as the mean, standard deviation, and coefficient of variation. These parameters collectively provide a comprehensive representation of the inter-nodal distance distribution, as outlined in equation 8. Following this step, the node-pair embeddings and inter-nodal distances are integrated with the predicted distribution to ascertain the likelihood that an inter-nodal distance mirrors that observed in the crystal conformation (formula 9). This resultant probability estimation can then be utilized as a scoring metric to evaluate the appropriateness of the current conformation in subsequent analyses.

$$\mu_{l,nl}, \sigma_{l,nl}, \pi_{l,nl} = \text{MDN_Block}(H_{l,nl}^1) \quad (8)$$

$$U_{(x)} = - \sum_{nl=1}^{NL} \sum_{l=1}^L \log P((d_{l,nl} | h_l, h_{nl})) = -score \quad (9)$$

where H represents the node embeddings; l, nl denote loop atoms and non-loop residues respectively; $\mu_{l,nl}, \sigma_{l,nl}, \pi_{l,nl}$ represent the means, standard deviations and mixing coefficients, respectively.

4.2 Post-processing

After KarmaLoop predicted the conformation, an optional Force Field (FF) optimization was implemented to remove unfavorable steric clashes and obtain high-quality loop conformations. OpenMM⁶⁴ was deployed for energy minimization by using the ff14SB force field to optimize the predicted conformation. To prevent significant changes to the protein, we applied a harmonic potential that restrains the backbone atoms (N, CA, C, and CB) to their original locations. Finally, we ran energy minimization on a GPU and saved the optimized protein structure to a new PDB file.

4.3 Benchmark dataset

The biennial Critical Assessment of protein Structure Prediction (CASP) is a worldwide contest for protein structure prediction, and is also commonly used for loop modeling assessment^{17,20,23,65}. The general loop benchmark consists of two datasets: CASP13+14 and CASP15. CASP13+14 is the combination of CASP13 and CASP14, which contains 549 loop structures from 52 proteins (the unmatched structure and sequence sample was removed). CASP15 containing 430 loop structures from 48 proteins was collected from the latest CASP competition. The antibody H3 benchmark derived from DeepAb is the combination of the RosettaAntibody and therapeutic benchmark⁶⁶, and comprises 92 antibody CDR H3 loop structures from 92 antibodies.

4.4 Training Dataset

In this study, the training data was collected from PDB and Structural Antibody Database (SAbDab)⁶⁷. The protein data from PDB was filtered by PISCES⁶⁸ using the following criteria: solved by X-ray crystallography, sequence identity $\leq 90\%$, resolution $< 3.0 \text{ \AA}$, R-factor ≤ 0.25 , and containing no DNA, RNA and UNK molecules. The non-secondary structure of PDB data was defined by DSSP⁶⁹ and we defined loops as regions connecting two secondary structures that consist of at least four residues. The antibody dataset was selected to be the same as that of DeepAb. The training and validation datasets were created using random stratified sampling according to the loop length in a 9:1 ratio. The antibody data was annotated using the Chothia numbering scheme⁷⁰. Specifically, the training data contain the CDR L1, L2, L3 H1, H2 and H3 regions, and each type of CDRs was also split following the 9:1 ratio, according to loop length. Finally, the total numbers of the data for training and validation are 250,257 and 27,832, respectively.

4.5 Dataset preprocessing

The protein data was downloaded from PDB, SAbDab and CASP. Water molecules were subsequently removed from the proteins, and the loop regions with non-standard amino acid residues or missing residues were removed. The pocket region was defined as the non-loop residues within 12 \AA of the loop atoms. Selecting the pocket instead of the entire protein can simplify the input of network and guide KarmaLoop to focus on the relevant structural features that are essential for understanding the interaction between loop and non-loop regions. Then, we initialized loop conformation by sampling from a normal distribution around the loop region.

4.6 Evaluation methods

In order to evaluate the performance of KarmaLoop, various widely-used traditional and DL methods were selected for comparison. The general protein loop modeling methods that were considered include (1) knowledge-based method: FREAD; (2) *ab initio* methods: DISGRO, NGK, and Rosetta-missing-loop (RML); (3) DL-based methods: AlphaFold and RoseTTAFold. According to the user guide, NGK requires a start conformation of loop region and if there is a missing loop, and RML can be used to fill it. In addition to these methods, several antibody structure prediction methods were also examined including DeepAb, RosettaAntibody-G⁶⁰, RepertoireBuilder⁶¹, and AbodyBuilder⁶² to assess the prediction ability of H3 loop region.

4.7 Metrics

For loop modeling tasks, it is essential to consider both accuracy and efficiency. Full-atom RMSD was utilized for evaluating the accuracy of prediction. KarmaLoop and traditional methods (FREAD, DISGRO, NGK and RML) focus solely on predicting the loop region of proteins, the RMSD values were then calculated directly based on the predicted conformations. Conversely, AlphaFold and RoseTTAFold model the entire protein structures, so that the predicted structures of protein are aligned before calculating RMSD values. Additionally, DeepAb, RosettaAntibody-G, RepertoireBuilder, and AbodyBuilder and RosettaAntibody predict the complete structure of antibodies. Following the same guidelines with DeepAb, the heavy chains of these antibodies are aligned prior to the RMSD calculation. Moreover, the success rate of the method was introduced as a complementary metric to RMSD, which measures the proportion of cases where the RMSD is less than or equal to 2 Å compared to experimentally determined conformations. The efficiency was simply measured by computing time.

4.8 Computing resource

KarmaLoop was trained on 8 NVIDIA A100-SXM4-80GB and 64 cores Intel(R) Xeon(R) Platinum 8358P CPU @ 2.60GHz. For evaluation, KarmaLoop was evaluated on a Tesla V100S GPU. Traditional methods (FREAD, DISGRO, NGK and RML) were accomplished in parallel with 48 cores Intel(R) Xeon(R) Gold 6240R CPU @ 2.40GHz. AlphaFold and RoseTTAFold were executed in parallel on 20 cores of the Intel(R) Xeon(R) Gold 6240R CPU @ 2.40GHz, and a Tesla V100S GPU.

Data and Code Availability

The source code will be available at <https://github.com/karma211225/KarmaLoop> once the paper is accepted.

Acknowledgments

This study was supported by the National Key Research and Development Program of China (2022YFF1203000), the National Natural Science Foundation of China (22220102001, 82204279, 22007082, 62006219), the Fundamental Research Funds for the Central Universities (226-2022-00220), Natural Science Foundation of Zhejiang Province (LQ21B030013) and Hong Kong Innovation and Technology Fund (Project No. ITS/241/21).

References

- 1 Tang, K., Zhang, J. & Liang, J. Fast protein loop sampling and structure prediction using distance-guided sequential chain-growth Monte Carlo method. *PLoS Comput Biol* **10**, e1003539 (2014).
- 2 Rufino, S. D., Donate, L. E., Canard, L. H. & Blundell, T. L. Predicting the conformational class of short and medium size loops connecting regular secondary structures: application to comparative modelling. *J Mol Biol* **267**, 352-367 (1997).

- 3 Lins, L., Thomas, A. & Brasseur, R. Analysis of accessible surface of residues in proteins. *Protein Science* **12**, 1406-1417 (2003).
- 4 Stevens, A. O. & He, Y. Benchmarking the Accuracy of AlphaFold 2 in Loop Structure Prediction. *Biomolecules* **12** (2022).
- 5 Lee, J., Lee, D., Park, H., Coutsias, E. A. & Seok, C. Protein loop modeling by using fragment assembly and analytical loop closure. *Proteins* **78**, 3428-3436 (2010).
- 6 Li, Z. *et al.* Flexibility Regulation of Loops Surrounding the Tunnel Entrance in Cytochrome P450 Enhanced Substrate Access Substantially. *ACS Catalysis* **12**, 12800-12808 (2022).
- 7 Crean, R. M., Biler, M., van der Kamp, M. W., Hengge, A. C. & Kamerlin, S. C. L. Loop Dynamics and Enzyme Catalysis in Protein Tyrosine Phosphatases. *Journal of the American Chemical Society* **143**, 3830-3845 (2021).
- 8 Borges, P. T. *et al.* Methionine-Rich Loop of Multicopper Oxidase McoA Follows Open-to-Close Transitions with a Role in Enzyme Catalysis. *ACS Catalysis* **10**, 7162-7176 (2020).
- 9 Jones, S. & Thornton, J. M. Prediction of protein-protein interaction sites using patch analysis. Edited by G. von Heijne. *J Mol Biol* **272**, 133-143 (1997).
- 10 Streaker, E. D. & Beckett, D. Ligand-linked Structural Changes in the Escherichia coli Biotin Repressor: The Significance of Surface Loops for Binding and Allostery. *J Mol Biol* **292**, 619-632 (1999).
- 11 Myllykoski, M., Raasakka, A., Han, H. & Kursula, P. Myelin 2',3'-cyclic nucleotide 3'-phosphodiesterase: active-site ligand binding and molecular conformation. *PLoS One* **7**, e32336 (2012).
- 12 Tamamis, P. & Floudas, Christodoulos A. Molecular Recognition of CXCR4 by a Dual Tropic HIV-1 gp120 V3 Loop. *Biophysical Journal* **105**, 1502-1514 (2013).
- 13 Papaleo, E. *et al.* The Role of Protein Loops and Linkers in Conformational Dynamics and Allostery. *Chem Rev* **116**, 6391-6423 (2016).
- 14 Zhao, S., Zhu, K., Li, J. & Friesner, R. A. Progress in super long loop prediction. *Proteins* **79**, 2920-2935 (2011).
- 15 Berman, H. M. *et al.* The Protein Data Bank. *Nucleic Acids Res* **28**, 235-242 (2000).
- 16 Marks, C. & Deane, C. M. Antibody H3 Structure Prediction. *Comput Struct Biotechnol J* **15**, 222-231 (2017).
- 17 Choi, Y. & Deane, C. M. FREAD revisited: Accurate loop structure prediction using a database search algorithm. *Proteins* **78**, 1431-1440 (2010).
- 18 Messih, M. A., Lepore, R. & Tramontano, A. LoopIng: a template-based tool for predicting the structure of protein loops. *Bioinformatics* **31**, 3767-3772 (2015).
- 19 Hildebrand, P. W. *et al.* SuperLooper--a prediction server for the modeling of loops in globular and membrane proteins. *Nucleic Acids Res* **37**, W571-W574 (2009).

- 20 Karami, Y., Guyon, F., De Vries, S. & Tufféry, P. DaReUS-Loop: accurate loop modeling using fragments from remote or unrelated proteins. *Sci Rep* **8**, 13673 (2018).
- 21 Barozet, A., Chacón, P. & Cortés, J. Current approaches to flexible loop modeling. *Curr Res Struct Biol* **3**, 187-191 (2021).
- 22 Marks, C. *et al.* Sphinx: merging knowledge-based and ab initio approaches to improve protein loop prediction. *Bioinformatics* **33**, 1346-1353 (2017).
- 23 Liang, S., Zhang, C. & Zhou, Y. LEAP: highly accurate prediction of protein loop conformations by integrating coarse-grained sampling and optimized energy scores with all-atom refinement of backbone and side chains. *J Comput Chem* **35**, 335-341 (2014).
- 24 Canutescu, A. A. & Dunbrack, R. L. Cyclic coordinate descent: A robotics algorithm for protein loop closure. *Protein Sci* **12**, 963-972 (2003).
- 25 Wang, C., Bradley, P. & Baker, D. Protein-protein docking with backbone flexibility. *J Mol Biol* **373**, 503-519 (2007).
- 26 Mandell, D. J., Coutsias, E. A. & Kortemme, T. Sub-angstrom accuracy in protein loop reconstruction by robotics-inspired conformational sampling. *Nature methods* **6**, 551-552 (2009).
- 27 Stein, A. & Kortemme, T. Improvements to robotics-inspired conformational sampling in rosetta. *PLoS One* **8**, e63090 (2013).
- 28 Deane, C. M. & Blundell, T. L. CODA: a combined algorithm for predicting the structurally variable regions of protein models. *Protein Sci* **10**, 599-612 (2001).
- 29 Deane, C. M. & Blundell, T. L. A novel exhaustive search algorithm for predicting the conformation of polypeptide segments in proteins. **40**, 135-144 (2000).
- 30 Deng, Y. *Deep learning on mobile devices: a review*. Vol. 10993 DCS (SPIE, 2019).
- 31 Jumper, J. *et al.* Highly accurate protein structure prediction with AlphaFold. *Nature* **596**, 583-589 (2021).
- 32 Baek, M. *et al.* Accurate prediction of protein structures and interactions using a three-track neural network. **373**, 871-876 (2021).
- 33 Lee, C., Su, B.-H. & Tseng, Y. J. Comparative studies of AlphaFold, RoseTTAFold and Modeller: a case study involving the use of G-protein-coupled receptors. *Brief Bioinform* **23** (2022).
- 34 Liang, T. *et al.* Differential performance of RoseTTAFold in antibody modeling. *Brief Bioinform* (2022).
- 35 LeCun, Y. *et al.* Backpropagation Applied to Handwritten Zip Code Recognition. *Neural Computation* **1**, 541-551 (1989).
- 36 Krizhevsky, A., Sutskever, I. & Hinton, G. E. ImageNet classification with deep convolutional neural networks. **60**, 84-90 (2017).

- 37 Zhang, N., Donahue, J., Girshick, R. & Darrell, T. 834-849 (Springer International Publishing).
- 38 Ouyang, W. *et al.* DeepID-Net: multi-stage and deformable deep convolutional neural networks for object detection. arXiv:1409.3505 (2014). <<https://ui.adsabs.harvard.edu/abs/2014arXiv1409.3505O>>.
- 39 He, K., Zhang, X., Ren, S. & Sun, J. in *IEEE Conference on Computer Vision and Pattern Recognition*.
- 40 Ruffolo, J. A., Guerra, C., Mahajan, S. P., Sulam, J. & Gray, J. J. Geometric potentials from deep learning improve prediction of CDR H3 loop structures. *Bioinformatics* **36**, i268-i275 (2020).
- 41 Gers, F. A., Schmidhuber, J. & Cummins, F. Learning to Forget: Continual Prediction with LSTM. *Neural Computation* **12**, 2451-2471 (2000).
- 42 Ruffolo, J. A., Sulam, J. & Gray, J. J. P. Antibody structure prediction using interpretable deep learning. **3**, 100406 (2022).
- 43 Abanades, B., Georges, G., Bujotzek, A. & Deane, C. M. ABlooper: fast accurate antibody CDR loop structure prediction with accuracy estimation. *Bioinformatics* **38**, 1877-1880 (2022).
- 44 Garcia Satorras, V., Hoogeboom, E. & Welling, M. J. a. e.-p. E(n) Equivariant Graph Neural Networks. arXiv:2102.09844 (2021). <<https://ui.adsabs.harvard.edu/abs/2021arXiv210209844G>>.
- 45 Liang, S., Zhang, C., Sarmiento, J. & Standley, D. M. Protein Loop Modeling with Optimized Backbone Potential Functions. *J Chem Theory Comput* **8**, 1820-1827 (2012).
- 46 Bonet, J., Segura, J., Planas-Iglesias, J., Oliva, B. & Fernandez-Fuentes, N. Frag'r'Us: knowledge-based sampling of protein backbone conformations for de novo structure-based protein design. *Bioinformatics* **30**, 1935-1936 (2014).
- 47 López-Blanco, J. R., Canosa-Valls, A. J., Li, Y. & Chacón, P. RCD+: Fast loop modeling server. *Nucleic Acids Res* **44**, W395-W400 (2016).
- 48 Chys, P. & Chacón, P. Random Coordinate Descent with Spinor-matrices and Geometric Filters for Efficient Loop Closure. *J Chem Theory Comput* **9**, 1821-1829 (2013).
- 49 Coutsiias, E. A., Seok, C., Jacobson, M. P. & Dill, K. A. A kinematic view of loop closure. *J Comput Chem* **25**, 510-528 (2004).
- 50 Gray, J. J. *et al.* Protein-Protein Docking with Simultaneous Optimization of Rigid-body Displacement and Side-chain Conformations. *J Mol Biol* **331**, 281-299 (2003).
- 51 Meiler, J. & Baker, D. ROSETTALIGAND: Protein-small molecule docking with full side-chain flexibility. **65**, 538-548 (2006).

- 52 Leach, A. R. Ligand docking to proteins with discrete side-chain flexibility. *J Mol Biol* **235**, 345-356 (1994).
- 53 Shen, C. *et al.* Boosting Protein–Ligand Binding Pose Prediction and Virtual Screening Based on Residue–Atom Distance Likelihood Potential and Graph Transformer. *Journal of Medicinal Chemistry* **65**, 10691-10706 (2022).
- 54 Morehead, A., Chen, C. & Cheng, J. J. a. e.-p. Geometric Transformers for Protein Interface Contact Prediction. arXiv:2110.02423 (2021). <<https://ui.adsabs.harvard.edu/abs/2021arXiv211002423M>>.
- 55 Dwivedi, V. P. & Bresson, X. J. a. e.-p. A Generalization of Transformer Networks to Graphs. arXiv:2012.09699 (2020). <<https://ui.adsabs.harvard.edu/abs/2020arXiv201209699D>>.
- 56 Jing, B., Eismann, S., Suriana, P., Townshend, R. J. L. & Dror, R. J. a. e.-p. LEARNING FROM PROTEIN STRUCTURE WITH GEOMETRIC VECTOR PERCEPTORS. arXiv:2009.01411 (2020). <<https://ui.adsabs.harvard.edu/abs/2020arXiv200901411J>>.
- 57 Kryshchuk, A., Schwede, T., Topf, M., Fidelis, K. & Moult, J. Critical assessment of methods of protein structure prediction (CASP)-Round XIII. *Proteins* **87**, 1011-1020 (2019).
- 58 Kryshchuk, A., Schwede, T., Topf, M., Fidelis, K. & Moult, J. Critical assessment of methods of protein structure prediction (CASP)—Round XIV. **89**, 1607-1617 (2021).
- 59 Luo, S. *et al.* Antigen-Specific Antibody Design and Optimization with Diffusion-Based Generative Models. 2022.2007.2010.499510 (2022).
- 60 Jeliak, J. R., Frick, R., Zhou, J. & Gray, J. J. Robustification of RosettaAntibody and Rosetta SnugDock. *PLoS One* **16**, e0234282 (2021).
- 61 Schmitt, D. *et al.* Repertoire Builder: high-throughput structural modeling of B and T cell receptors. *Molecular Systems Design & Engineering* **4**, 761-768 (2019).
- 62 Dunbar, J. *et al.* SAbPred: a structure-based antibody prediction server. *Nucleic Acids Res* **44**, W474-W478 (2016).
- 63 Jin, W., Barzilay, R. & Jaakkola, T. J. a. e.-p. Antibody-Antigen Docking and Design via Hierarchical Equivariant Refinement. arXiv:2207.06616 (2022). <<https://ui.adsabs.harvard.edu/abs/2022arXiv220706616J>>.
- 64 Eastman, P. *et al.* OpenMM 4: A Reusable, Extensible, Hardware Independent Library for High Performance Molecular Simulation. *J Chem Theory Comput* **9**, 461-469 (2013).
- 65 Lee, G. R., Heo, L. & Seok, C. Effective protein model structure refinement by loop modeling and overall relaxation. *Proteins* **84 Suppl 1**, 293-301 (2016).
- 66 Raybould, M. I. J. *et al.* Five computational developability guidelines for therapeutic antibody profiling. **116**, 4025-4030 (2019).

- 67 Dunbar, J. *et al.* SAbDab: the structural antibody database. *Nucleic Acids Res* **42**, D1140-D1146 (2013).
- 68 Wang, G. & Dunbrack, R. L. PISCES: recent improvements to a PDB sequence culling server. *Nucleic Acids Res* **33**, W94-W98 (2005).
- 69 Touw, W. G. *et al.* A series of PDB-related databanks for everyday needs. *Nucleic Acids Res* **43**, D364-D368 (2015).
- 70 Chothia, C. *et al.* Conformations of immunoglobulin hypervariable regions. *Nature* **342**, 877-883 (1989).